The International Journal of Advanced Manufacturing Technology (2019) 103:1279–1290
https://doi.org/10.1007/s00170-019-03535-2

ORIGINAL ARTICLE

Optimization of hard turning process parameters using the response surface methodology and finite element simulations

S. Arfaoui [1] · F. Zemzemi [1] · M. Dakhli [1] · Z. Tourki [1]

Received: 20 December 2018 / Accepted: 1 March 2019 / Published online: 3 April 2019

Abstract
Hard turning is a manufacturing process widely used in aerospace industries. The effect of hard turning on the surface integrity is mainly influenced by the choice of the process parameters. The aim of this paper is to present an exhaustive study for optimizing the hard turning process parameters using the response surface methodology (RSM) coupled with the finite element method. In particular, a case study is developed where AISI 52100 (62 HRc) is machined by PCBN tool. For this purpose, a finite element model (FEM) of orthogonal cutting is developed by the software ABAQUS. In this study, empirical models of machining forces and white layers (WL) thickness are developed. The empirical models have been determined using the RSM, in which three factors with three levels are implemented. The cutting speed, the feed rate, and the depth of cut are considered as the main input parameters. The analysis of variance (ANOVA) was also employed in order to analyze the effects and interactions of the cutting parameters on the performance of machined parts. Lastly, the optimum parametric combination is determined to allow the minimization of machining forces and WL thickness. The proposed approach can be considered as a helpful method for engineering design to optimize hard turning parameters.

Keywords Response surface methodology · Finite element modeling · Hard turning · Machining forces · White layers thickness

1 Introduction

The hard turning improved the manufacturing process by giving potential advantages comparing to conventional grinding. The reduced costs, the few process steps, the possibility of operating without coolants, and the high geometrical flexibility can be identified as the main advantages offered by hard turning.

Frequently, scientific researchers are interested in studying the hard turning process in terms of residual stresses [1], surface roughness [2], cutting forces [3], and white layers (WL) formation [4]. It was well illustrated that hard turning results are extremely dependent on the cutting process conditions (cutting speed, feed rate, tool geometry, workpiece hardness, etc.). Yan et al. [5] showed that the increase of the nose radius, the feed rate, and the depth of cut induces an increase of the machining forces in hard turning of AISI H13 steel. Similar observations were revealed in hard turning of other steels such as AISI D2 [6]. Zhang et al. [7] investigated the effect of various process parameters on machining forces and WL thickness. They found that increasing the workpiece hardness, the feed rate, and the cutting speed induces an increase of the WL thickness in machined samples and that the machining forces have a decreasing tendency with the rise of cutting speed. Arfaoui et al. [8] illustrated that the WL thickness is increased with higher tool flank wear, higher cutting speed, and feed rate.

Nevertheless, the aforementioned studies cannot be used to optimize the hard turning process since they do not take into account the combined effect of process parameters. In this context, the response surface methodology (RSM) has become a topic of interest for engineering designer in industrial application thanks to its ability to consider the influences and interactions of all process parameters. Consequently, many predictive approaches were proposed. Saiini et al. [9] developed an empirical linear model for tool wear and a nonlinear model for surface roughness in hard turning of AISI H11 steel. They conducted twenty-nine tests considering the cutting speed, the feed rate, and the depth of cut as process parameters. The same output results (tool wear and surface roughness) were

✉ S. Arfaoui
arfaoui.samar@gmail.com

[1] Laboratory of Mechanics of Sousse, National Engineering School of Sousse, University of Sousse, BP 264 Erriadh, 4023 Sousse, Tunisia

investigated in hard turning of AISI 4140 steel [10]. The authors used a full factorial design and the analysis of variance (ANOVA) to prove that the surface roughness is influenced mainly by the feed rate. Whereas the tool wear is affected by the cutting speed and the interaction between the depth of cut and the feed rate. Lalwani et al. [11] used the RSM to provide an empirical model describing the relationship between surface roughness, machining forces, and cutting parameters (cutting speed, feed rate, and depth of cut). Bouacha et al. [12] presented a study of surface roughness and cutting forces evolution in hard turning of AISI52100 steel. The obtained results showed that the feed rate and the cutting speed mainly affect the surface roughness while the cutting forces are mainly influenced by the depth of cut. The authors used the response surface optimization in order to identify the optimal combination of cutting parameters to obtain better surface finish quality in the hard turning process. Ozel et al. [13] conducted a set of two-level fractional experiments using the hardness, the edge geometry, the feed rate, and the cutting speed as factors. The ANOVA results reported the influences of parameters on the surface roughness and the cutting forces in finish hard turning of AISI H13 steel.

Although many contributions were made dealing with the RSM in hard turning process, the RSM is not yet applied on optimizing both machining forces and WL thickness. The aim of this paper is to optimize the machining process performance, machining forces and WL thickness, through controlling the cutting conditions. The design of experiments (DoE) with three levels is implemented in order to investigate the effect and the interaction between the different factors (cutting speed, feed rate, and depth of cut) on the cutting forces and WL thickness.

The overall suggested approach consists in the following:

(i) Development of an orthogonal cutting model of a hardened steel by means of finite element method.
(ii) Modeling of WL thicknesses based on the phase transformations mechanism by taking into account the mechanical effect to the austenitic transformation temperature.
(iii) Generating of DoE methodology and providing empirical models for thrust forces, cutting forces, and WL thickness.
(iv) Optimizing the hard turning conditions.

2 Background of the response surface methodology

RSM is a powerful method used in analyzing problems in which the objective is to optimize the response. The methodology consists in a set of statistical and mathematical tools established between desired responses and independent input variables [14].

These designs are able to construct a polynomial approximation of the response based on the results given by the DoE method where a full factorial design plan is implemented. In the case of the nonlinear (quadratic) response surface with three variables, the response is written as follows:

$$Y = b_0 + \sum_{i=1}^{K} b_i X_i + \sum_{i=1}^{K} b_{ii} X_i^2 + \sum_{ij}^{K} b_{ij} X_i X_j \quad (1)$$

where X_i represents the input parameters and the coefficients b_0, b_i, b_{ii}, and b_{ij} are the free terms of the regression equation, the linear effect of X_i, the quadratic effect of X_i^2, and the linear-by-linear interaction between X_i and X_j, respectively.

3 Finite element modeling of orthogonal cutting

The FE simulations of orthogonal cutting are performed using the commercial FE software ABAQUS 6.10. The explicit solver is used in all calculations in order to consider the dynamic effects generated by material forming operations. A fully coupled thermal-stress analysis is performed to reproduce the thermo-mechanical behavior of machined steels.

3.1 Geometry, boundary conditions, and mesh

The geometric model is composed by two bodies: the tool (part1) and the workpiece as illustrated in Fig. 1. The workpiece is modeled as a multi-part rectangle (1.5 mm width × 5 mm long) including the chip (part2), the separation layer (part3), and the base (part4). The whole model is meshed with 21092 quadrilateral elements of type four-node bilinear displacement and temperature (CPE4RT). The cutting speed is applied to the tool along the X-axis while both left and bottom surfaces of the base are fixed. The mesh density is dependent to the regions of the geometric model. In fact, a refined mesh (1 μm) is implemented along the tool-workpiece contact area and in the top of machined material but far away from the interaction zone; the workpiece is marginally affected by the tool loadings; therefore, a coarser mesh is sufficient in the bottom side.

3.2 Constitutive equations

3.2.1 Mechanical behavior

A thermo-elasto-viscoplastic flow stress is mandatory to describe the material behavior of the steel during machining process. In this propose, the Johnson-Cook [15] model is

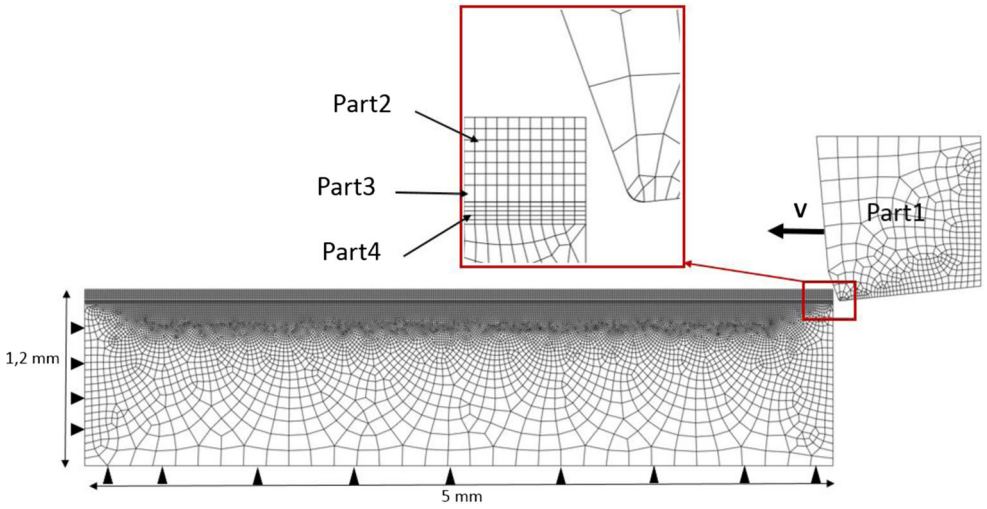

Fig. 1 The orthogonal cutting model

implemented as an isotropic hardening. The model is described as a function of three distinctive terms (strain, strain rate, and temperature).

$$\overline{\sigma} = \left(A + B\left(\overline{\varepsilon_p}\right)^n\right)\left(1 + C\ln\left(\frac{\dot{\overline{\varepsilon_p}}}{\dot{\overline{\varepsilon}}_0}\right)\right)\left(1-\left(\frac{T-T_0}{T_m-T_0}\right)^m\right) \quad (2)$$

where $\overline{\sigma}$, $\overline{\varepsilon_p}$, $\dot{\overline{\varepsilon}}_p$, $\dot{\overline{\varepsilon}}_0$, T, T_m, and T_0 are equivalent flow stress, equivalent plastic strain, equivalent plastic strain rate, reference strain rate, temperature, melting temperature, and ambient temperature, respectively. The material constant A is the yield strength, B is the hardening modulus, C is the strain rate sensitivity, n is the strain hardening exponent, and m is the thermal softening exponent.

3.2.2 Damage criterion

In order to simulate the chip formation, the Johnson-Cook damage criterion is implemented in the FE code. The criterion is expressed as a cumulative damage law as follows:

$$D_m = \sum \frac{\overline{\Delta\varepsilon_p}}{\overline{\varepsilon_f}} \quad (3)$$

when the equality between the equivalent plastic strain "$\overline{\Delta\varepsilon_p}$" and the equivalent strain at failure "$\overline{\varepsilon_f}$" is achieved and the damage "D_m" reaches the value of one. Thus, the corresponding elements will be deleted allowing the separation of the chip from the workpiece.

The equivalent strain at failure is expressed as follows:

$$\overline{\varepsilon_f} = [D_1 + D_2\exp(D_3\eta)] \times \left[1 + D_4\ln\left(\frac{\dot{\overline{\varepsilon_p}}}{\dot{\overline{\varepsilon}}_0}\right)\right] \times \left[1 + D_5\left(\frac{T-25}{T_m-25}\right)\right] \quad (4)$$

where $D_1 - D_5$ are the Johnson-Cook damage parameters and η is the stress triaxiality parameter.

3.2.3 Heat generation and friction

In the current work, the heat is considered deriving from friction and inelastic energy dissipation. The quantity of the energy converted into heat and deriving from plastic strain and friction contact is described through Eqs. (5) and (6), respectively.

$$\dot{q}_p = \eta_p \bar{\sigma} : \dot{\overline{\varepsilon_p}} \quad (5)$$

$$\dot{q}_f = \eta_f \tau : v_g \quad (6)$$

where η_p is the Taylor-Quinney coefficient representing the inelastic heat fraction which is often equal to 0.9 for metallic materials and means that 90% of the plastic work is converted into heat. The η_f is often equal to one and means that the total friction work is converted into heat. The interaction between the tool-workpiece is defined between the outer surface of the tool and the nodes of the workpiece. The contact is characterized by the Coulomb friction law.

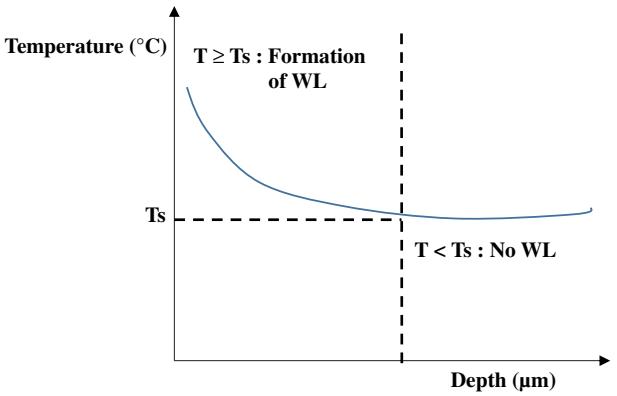

Fig. 2 Procedure adopted for modeling the white layer

Table 1 Material properties of AISI52100 (62HRc) and PCBN tool

Property	Workpiece (AISI52100)	Tool (PCBN)
Density (kg·m^{-3})	7827	3120
Inelastic heat fraction	0.9	×
Conductivity (W·m^{-1}·K^{-1})	43 − 0.0298T	100
Specific heat (J·kg^{-1}·K^{-1})	458 + 0.504T	960
Young's modulus (GPa, °C)	(201.3,25); (178.5,200); (162.7,400); (103.2,600); (86.87,800); (66.88,1000)	680
Poisson's ratio (°C)	(0.227,25); (0.269,200); (0.255,400); (0.342,600); (0.396,800); (0.49,1000)	0.22
Thermal expansion (× 10^{-6} °C^{-1}, °C)	(11.5,25); (12.6,204); (13.7,398); (14.9,704); (15.3,804)	4.9

3.2.4 Modeling of white layers thickness

WL are a microstructural state resulting from phase transformations mechanism. The presence of the retained austenite in machined samples is an indicator for the occurrence of an austenitic transformation during the tool passage. Predicting the WL thicknesses is based on comparing the simulated temperature in the machined workpiece (temperature beneath machined surface) to the austenitic transformation temperature (Ts). The WL are located in the surface of the machined workpiece where the simulated temperatures are higher than Ts.

The austenitic transformation temperature is extracted from the CCT diagrams of steels. These diagrams are established in quasi-static conditions where mechanical effects are not considered. However, stress and strain strongly contribute in machining process. Thus, in the current work, mechanical effects are tacked into account by the use of the chemical equilibrium potentials established between ferrite/martensite (m) phase and austenite (a) [16]. In fact, the chemical equilibrium potentials established between martensite phase (α) and austenite phase (γ) at condition (T, P) are modeled as follows:

$$G^{\alpha}{}_{m} = G^{\gamma}{}_{m} \tag{7}$$

At the condition (dT, dP), the chemical equilibrium potentials are expressed as follows:

$$dG^{\alpha}{}_{m} = dG^{\gamma}{}_{m} \tag{8}$$

Since the phase transformation from martensite into austenite is endothermic and absorbing the strain energy, then the thermodynamic equations can be expressed as follows:

$$dG^{\alpha}{}_{m} = -S^{\alpha}{}_{m}dT + V^{\alpha}{}_{m}dP + dW_{s} \tag{9}$$

$$dG^{\gamma}{}_{m} = -S^{\gamma}{}_{m}dT + V^{\gamma}{}_{m}dP \tag{10}$$

Combining equations (8), (9), and (10), the following equation can be obtained:

$$\Delta^{\gamma}_{\alpha}S_{m}dT = \Delta^{\gamma}_{\alpha}V_{m}dP - dW_{s} \tag{11}$$

The chemical potential of the two phases can be also modeled as follows:

$$G^{\alpha}{}_{m} = H^{\alpha}{}_{m} - TS^{\alpha}{}_{m} \tag{12}$$

$$G^{\gamma}{}_{m} = H^{\gamma}{}_{m} - TS^{\gamma}{}_{m} \tag{13}$$

Considering that ΔG is equal to zero when the reversible transformation occurs, the molar entropy increment can be described as follows:

$$\Delta^{\gamma}_{\alpha}S_{m} = \Delta^{\gamma}_{\alpha}H_{m}/T \tag{14}$$

Consequently, from the equality between Eqs. (11) and (14), the following equation can be obtained:

$$\Delta^{\gamma}_{\alpha}V_{m}dP - dW_{s} = \left(\Delta^{\gamma}_{\alpha}H_{m}/T\right)dT \tag{15}$$

Finally, we obtain the expression of the austenitic transformation temperature (Ts) by integrating the previous equation:

$$Ts = Ts_{CCT}\exp\left(\Delta^{a}_{m}V.P - W_{s}\right)/\Delta^{a}_{m}H \tag{16}$$

where $\Delta^{a}_{m}V$ is the molar volume increment during phase transformation, $\Delta^{a}_{m}H$ is the molar enthalpy of phase transformation, and Ts_{CCT} is the austenitic transformation temperature extracted from CCT diagrams without taking into account the mechanical effects.

The value of simulated temperature (T), equivalent stress (P), and strain energy (W_s) is extracted from the machined workpiece. As mentioned earlier, if the simulated temperature exceeds the calculated austenitic transformation temperature (Ts), then an austenitic transformation occurs and the WL

Table 2 Johnson-cook constants of AISI52100 (62HRc)

A (MPa)	B (MPa)	C	n	m	D1	D2	D3	D4	D5
2482.4	1498.5	0.027	0.19	0.66	0.0368	2.34	− 1.484	0.0035	0.411

Table 3 Levels of input factors

Parameters	Notations	Levels		
		− 1	0	1
Cutting speed (m/min)	V	100	200	300
Feed (mm/rev)	f	0.05	0.1	0.15
Depth of cut (mm)	d	1	2.5	4

thickness is assumed to be equal to the depth of the austenized zone. If the simulated temperature in the machined surface is lower than the austentic transformation temperature (Ts), then no WL are formed. The procedure of modeling the WL is summarized in Fig. 2.

4 Application

In this study, an application has been carried out on the hardened steel: AISI 52100 (62 HRc). This material is a hypereutectoid low-alloy steel machined by a Polycrystalline Cubic Boron Nitride (PCBN) tool. The thermo-mechanical properties of these materials are mentioned in Table 1 [17]. The Johnson-Cook hardening and damage parameters (A, B, n, C, m, and Di) of AISI 52100 are represented in Table 2 [18]. The Ts_{CCT} is equal to 750 °C according to the CCT diagram of the chosen steel [19], $\Delta_m^a V$ is equal to − 0.06 $cm^3 \cdot mol^{-1}$, and $\Delta_m^a H$ is equal to 920.5 $J \cdot mol^{-1}$.

4.1 Application 1: validation of the finite element model (FEM)

In order to check the accuracy of the proposed FEM, different cutting conditions are adopted from previous experimental investigations [7]. The orthogonal cutting process is performed on a CNC lathe under dry conditions. The tool is a CBN insert mounted on the tool-holder (STFCR2525M16, KENNAMETAL). The geometric characteristics of the cutting edge are a chamfer land of 0.1 mm × 15°, a cutting edge

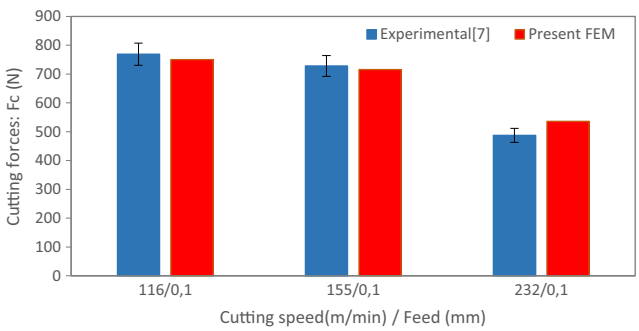

Fig. 3 Comparison of predicted and experimental cutting forces

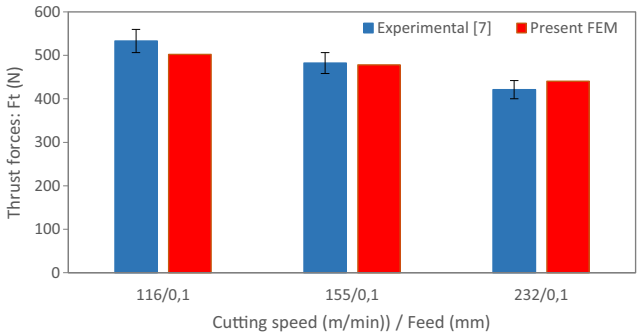

Fig. 4 Comparison of predicted and experimental thrust forces

radius of 20 μm, a clearance angle of 7°, and a rake angle of 0°.

The depth of cut is kept constant at 2.5 mm; two feed rates (0.075 mm/rev and 0.1 mm/rev) and three cutting speeds (116 m/min, 155 m/min, and 232 m/min) are employed. The contact between the tool and the workpiece is modeled by the Coulomb friction model with a 0.35 friction coefficient [20].

4.2 Application 2: optimization of cutting conditions

The DOE is utilized to study the relationship between the desired response (machining forces and WL thickness) and the input parameters. It requires twenty-seven tests where three factors are used at three levels. The factors employed in the current work are the feed rate, the cutting speed, and the depth of cut. Each factor is varied at lowest (− 1), middle (0), and highest (1) levels. Table 3 shows the factors and their levels in actual and coded values. The design is generated and analyzed with the software MINITAB 16.0.

5 Results

5.1 Validation

The comparisons between the experimentally measured [7] and numerically predicted cutting and thrust forces are represented in Figs. 3 and 4, respectively. The forces in the cutting direction are higher than those in the feed direction. This finding is in correlation with the experimental trend. The obtained results show a good agreement with the experimental ones since the average error percentage is almost 5% in the cutting forces and 4% in the thrust ones. These errors can be associated with the dispersion of material properties.

Figure 5 exhibits the prediction of WL thickness in the machined workpiece. The thickness corresponds to the intersection between the simulated temperature (temperature beneath machined surface) and the austenitic transformation temperature (*T*s). The simulated temperature is calculated through a path in the machined workpiece just beneath the tool passage and it has a decreasing profile. This is due to

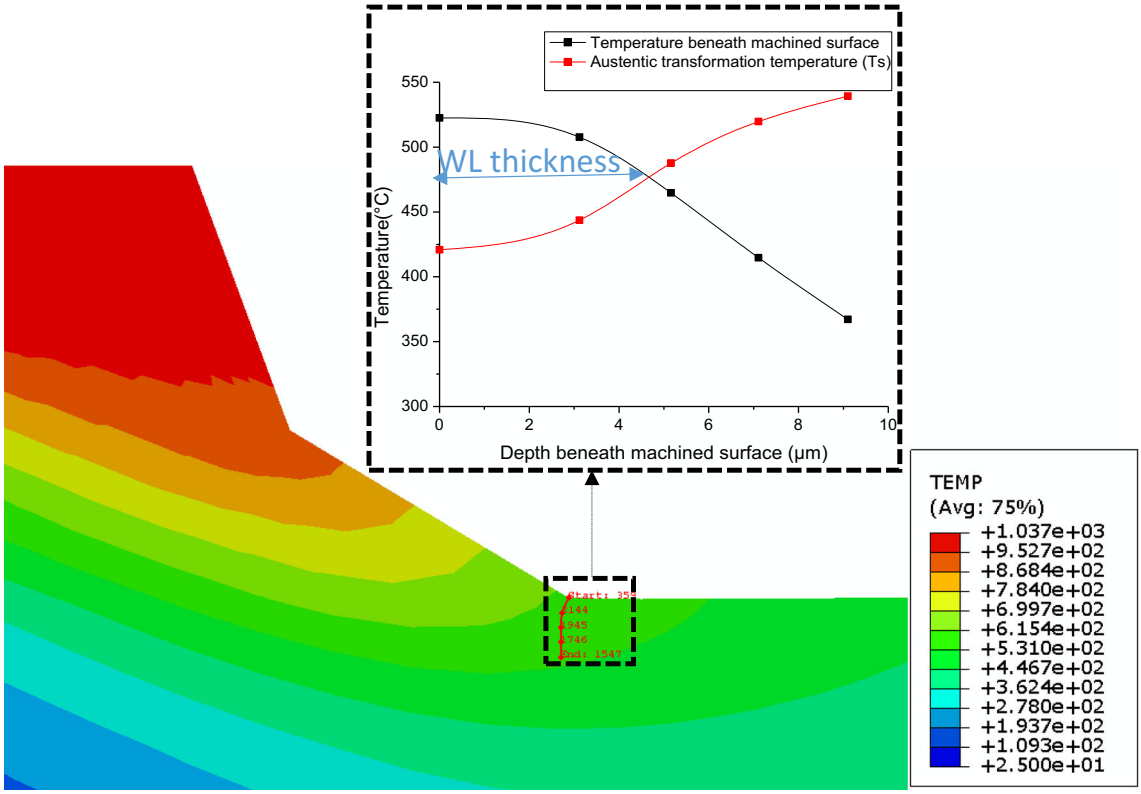

Fig. 5 Prediction of white layers thickness in the machined workpiece

the heat distribution in cutting operation. In fact, the heat is maximized at the surface where the quantity of friction and inelastic energy are important and minimized far away from the surface where friction and inelastic energy are marginal. The austenitic transformation temperature has an increasing profile which is explained by Eq. (16).

The simulated results of WL thickness under three cutting conditions are compared to the experimental data [7] and plotted in Fig. 6. The efficiency of the adopted method is approved since the average error is equal to 7.65%. It is also noticed that the little discrepancy between numerical simulations and experimental measurements can be associated with the dispersion of material properties which is not tacked into account in this study.

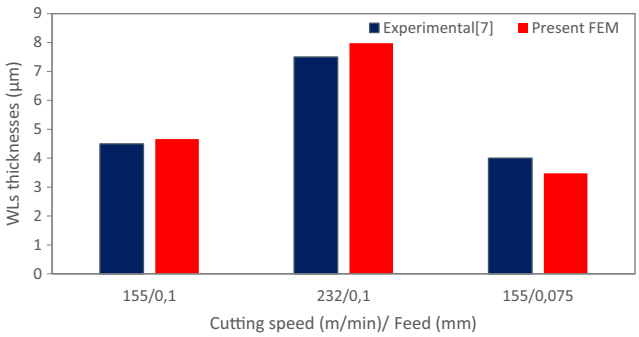

Fig. 6 Comparison of predicted and experimental white layers thickness

5.2 Development of empirical models

In this section, empirical models are proposed to estimate the WL thickness and the machining (cutting and thrust) forces. The relationships between input parameters (cutting speed,

Table 4 Analysis of variance for white layers thickness

Source	DF	Seq SS	Adj SS	Adj MS	F	P
Regression	9	490.873	490.873	54.541	366.70	0.000
Linear	3	481.512	481.512	160.504	1079.11	0.000
f	1	299.064	299.064	299.064	2010.70	0.000
V	1	180.057	180.057	180.057	1210.57	0.000
d	1	2.391	2.391	2.391	16.07	0.001
Square	3	1.581	1.581	0.527	3.54	0.037
f*f	1	1.483	1.483	1.483	9.97	0.006
V*V	1	0.092	0.092	0.092	0.62	0.442
d*d	1	0.006	0.006	0.006	0.04	0.846
Interaction	3	7.780	7.780	2.593	17.44	0.000
f*V	1	7.632	7.632	7.632	51.31	0.000
f*d	1	0.030	0.030	0.030	0.20	0.659
V*d	1	0.118	0.118	0.118	0.79	0.386
Residual error	17	2.529	2.529	0.149		
Total	26	493.402				

Table 5 Analysis of variance for cutting forces

Source	DF	Seq SS	Adj SS	Adj MS	F	P
Regression	9	4475337	4475337	497260	177.00	0.000
Linear	3	4127416	4127416	1375805	489.71	0.000
f	1	799892	799892	799892	284.71	0.000
V	1	220556	220556	220556	78.51	0.000
d	1	3106968	3106968	3106968	1105.90	0.000
Square	3	62934	62934	20978	7.47	0.002
f*f	1	60675	60675	60675	21.60	0.000
V*V	1	2259	2259	2259	0.80	0.382
d*d	1	0	0	0	0.00	0.994
Interaction	3	284987	284987	94996	33.81	0.000
f*V	1	39425	39425	39425	14.03	0.002
f*d	1	193492	193492	193492	68.87	0.000
V*d	1	52070	52070	52070	18.53	0.000
Residual error	17	47761	47761	2809		
Total	26	4523098				

feed rate, and depth of cut) and desired responses are developed based on the RSM results, as follows:

(i) The cutting forces (Fc) model is given by Eq. (17) in which the determination coefficient (R^2) is 98.94%:

$$F_c = 613.83 + 210.80\ \mathrm{f} - 110.69\ \mathrm{V} + 415.46\ \mathrm{d} + 100.56\ \mathrm{f}^2 + 19.40\ \mathrm{V}^2 + 0.1768\ \mathrm{d}^2 - 57.31\ \mathrm{f} \times \mathrm{V} + 126.98\ \mathrm{f} \times \mathrm{d} - 65.87\ \mathrm{V} \times \mathrm{d} \quad (17)$$

(ii) The thrust forces (Ft) model is given by Eq. (18) in which the determination coefficient (R^2) is 99.61%:

$$F_t = 468.96 + 71.13\ \mathrm{f} - 28.26\ \mathrm{V} + 298.74\ \mathrm{d} + 44.95\ \mathrm{f}^2 + 0.6942\ \mathrm{V}^2 + 0.5785\ \mathrm{d}^2 - 11.38\ \mathrm{f} \times \mathrm{V} + 43.32\ \mathrm{f} \times \mathrm{d} - 16.81\ \mathrm{V} \times \mathrm{d} \quad (18)$$

Table 6 Analysis of variance for thrust forces

Source	DF	Seq SS	Adj SS	Adj MS	F	P
Regression	9	1751545	1751545	194616	483.14	0.000
Linear	3	1711939	1711939	570646	1416.64	0.000
f	1	91071	91071	91071	226.08	0.000
V	1	14376	14376	14376	35.69	0.000
d	1	1606492	1606492	1606492	3988.14	0.000
Square	3	12131	12131	4044	10.04	0.000
f*f	1	12126	12126	12126	30.10	0.000
V*V	1	3	3	3	0.01	0.933
d*d	1	2	2	2	0.00	0.945
Interaction	3	27476	27476	9159	22.74	0.000
f*V	1	1554	1554	1554	3.86	0.066
f*d	1	22527	22527	22527	55.92	0.000
V*d	1	3394	3394	3394	8.43	0.010
Residual error	17	6848	6848	403		
Total	26	1758393				

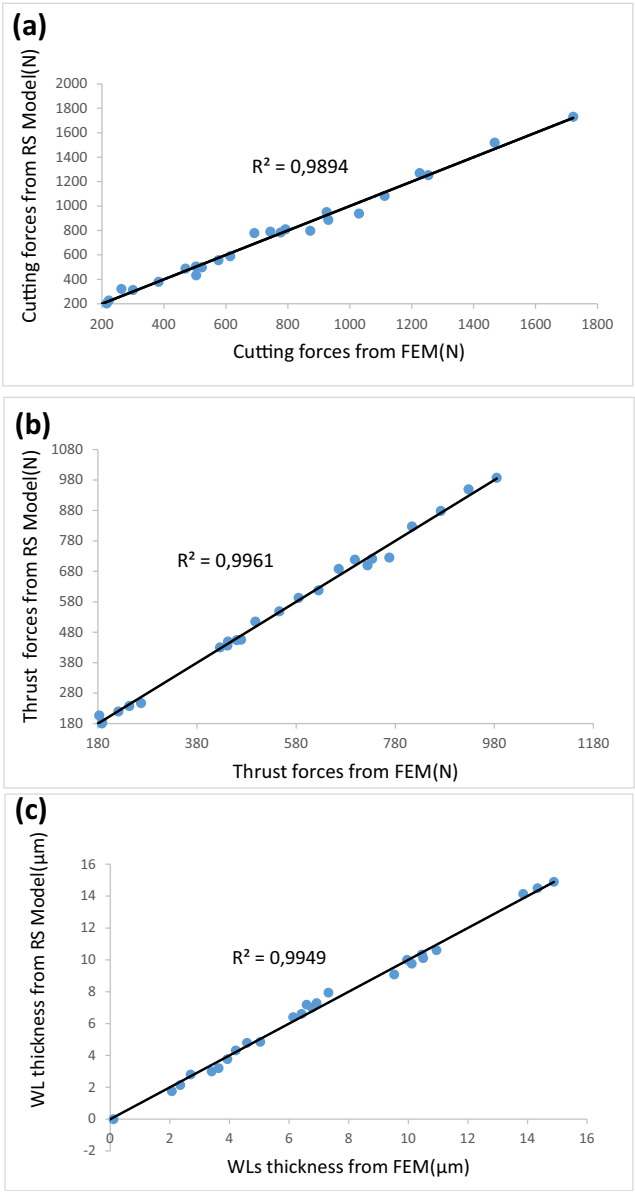

Fig. 7 Goodness of fit of RS model for cutting forces (**a**), thrust forces (**b**), and white layers thickness (**c**)

(iii) The WL model is given by Eq. (19) in which the determination coefficient (R^2) is 99.49%:

$$WLs = 6.92 + 4.07\ \mathrm{f} + 3.16\ \mathrm{V} - 0.364\ \mathrm{d} - 0.497\ \mathrm{f}^2 - 0.123\ \mathrm{V}^2 + 0.031\ \mathrm{d}^2 + 0.797\mathrm{f} \times \mathrm{V} - 0.05\ \mathrm{f} \times \mathrm{d} - 0.099\ \mathrm{V} \times \mathrm{d} \quad (19)$$

Furthermore, the ANOVA tables of the analytical models for the desired responses are represented in Tables 4, 5, and 6. The tables illustrate that the P values of the linear effects are significant for WL thickness, cutting forces, and thrust forces. Statistically, P values decide whether the parameters are significantly different. A minimum P value (less than 0.05) shows the greater impact on the machining characteristics. Minimum P values are

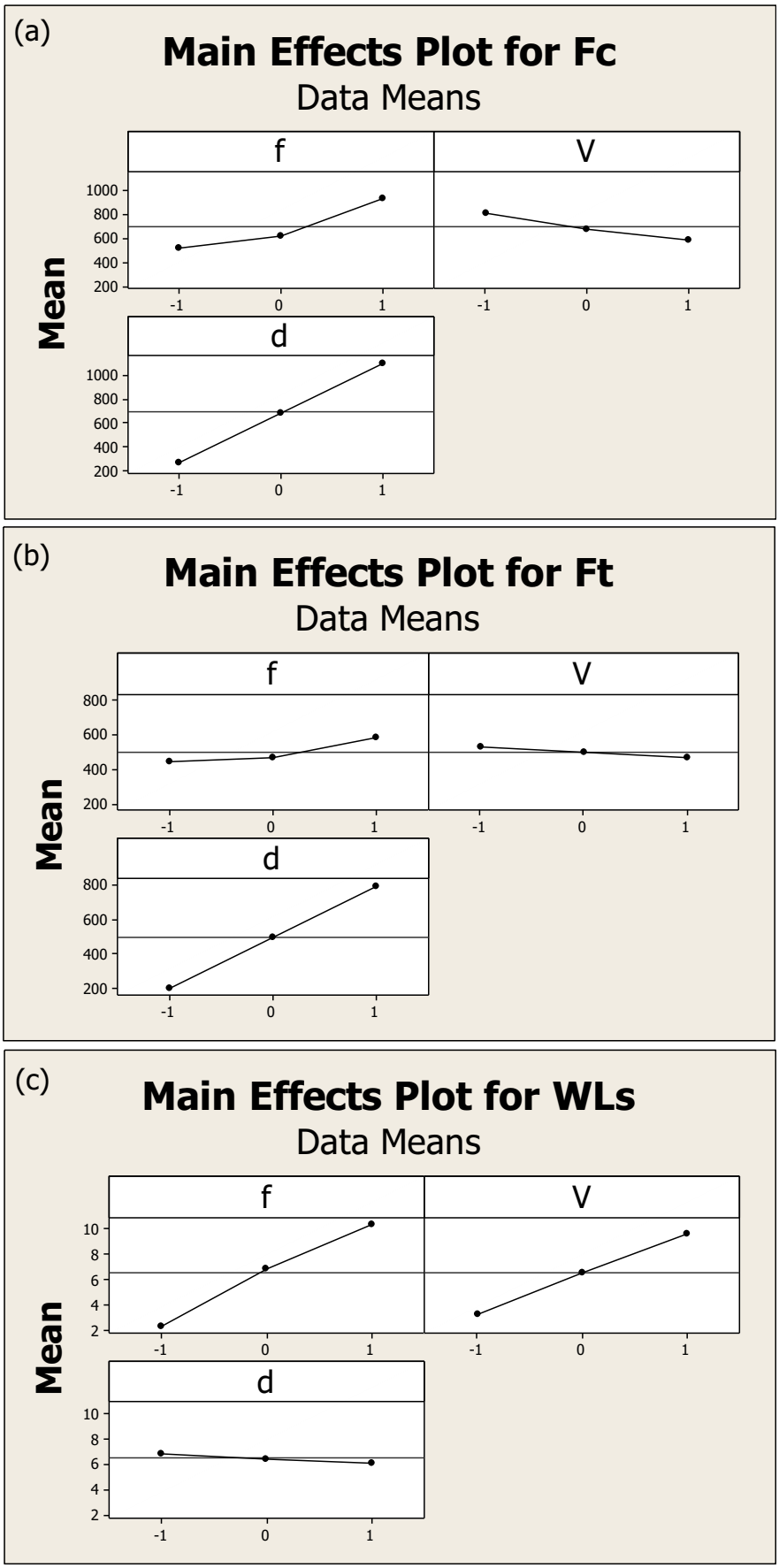

Fig. 8 Main effect plot of cutting parameters on the Fc (**a**), main effect plot of cutting parameters on the Ft (**b**), main effect plot of cutting parameters on the WL thickness (**c**), interaction effect plot of cutting parameters on the Fc (**d**), interaction effect plot of cutting parameters on the Ft (**e**), interaction effect plot of cutting parameters on the WL thickness (**f**)

Fig. 8 (continued)

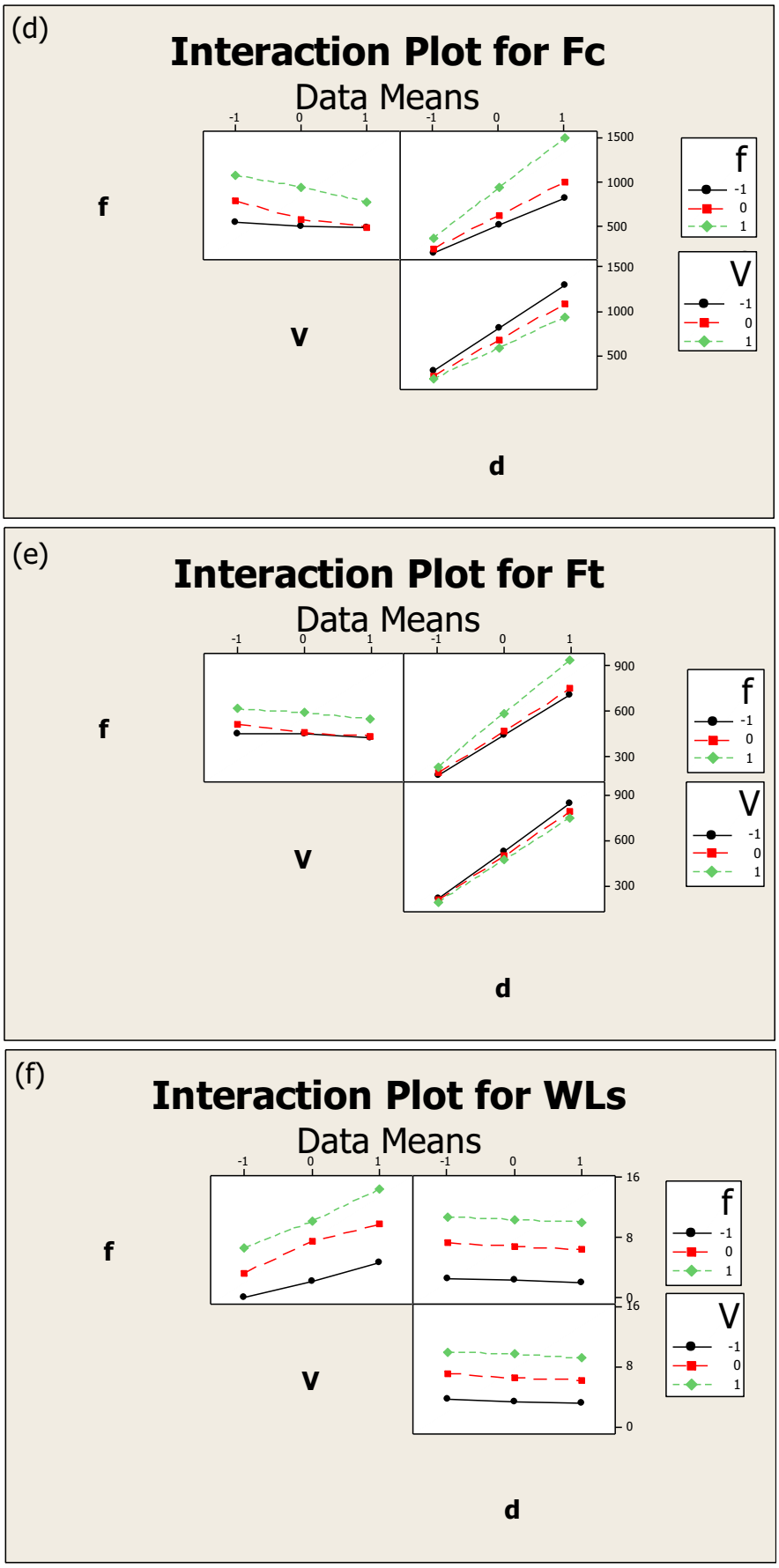

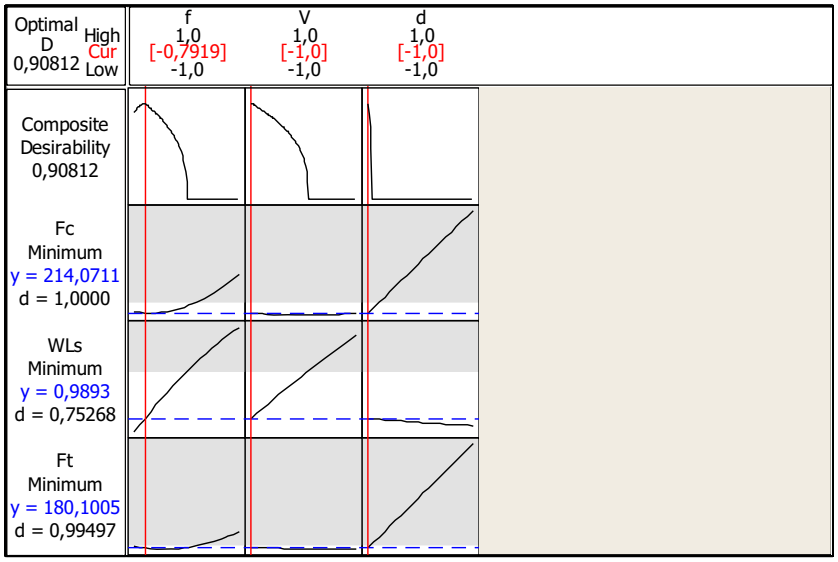

Fig. 9 Simultaneous optimization of cutting forces and white layers thickness

observed for feed and cutting speed in the area of WL depth. For the machining forces, the depth of cut, the feed, and the cutting speed have minimum *P* values.

A twenty-seven verification points are generated so as to assure the accuracy of the established RS model. The obtained results plotted in Fig. 7 indicate that the model is highly reliable in predicting WL thickness and machining forces. In fact, the high value of *R*-squared (almost 99%) reveals the efficiency of the developed empirical relationships.

The empirical models developed in this section allow calculating the thickness of the white layers and the values of the machining forces from knowing only the cutting conditions (cutting speed, feed rate, and depth of cut).

5.3 Effect and sensitivity analysis of input factors

The DOE which is used to investigate both the main and the interaction effects of input parameters on the machining forces and WL thickness is presented by the response graphs in Fig. 8. It is worth noticing that all selected parameters have an influence on the desired responses. Figure 8 (a) and (b) show the main effect of input factors on the cutting and thrust forces. It can be deduced that the depth of cut is the principal factor influencing the machining forces. Indeed, it is seen that the machining forces increase with the increase of the depth of cut as well as the feed rates. In fact, increasing those parameters makes the cutting zone greater. Thus, a rise of machining forces is required for chip formation. Nevertheless, high cutting speeds lead to lower machining forces. In fact, increasing the speed generates high cutting temperatures. Thus, a thermal softening of the workpiece occurs which make the forces needed for the material cutting become weaker.

Figure 8 (c) exhibits the main effect of the input factors on WL thickness induced by hard turning process. The WL depth is affected by every parameter to some degree. The dominant factors are the cutting speed and the feed. It is illustrated that increasing the feed rates and the cutting speeds enhances the thicknesses of the WL. In fact, the rise of the cutting conditions leads to higher temperatures in the machined material [21, 22]. Therefore, deeper austenized depths are induced and thicker WL is formed. The same figure shows that the WL thickness decreases slightly with the rise of the depth of cut. This effect could be explained by the reduced distance between the shear plane and the workpiece. Consequently, the influenced area of the heat source is reduced and the WL thickness decreases. At high feed (0.15 mm in the experiment), the maximum forces and WL thicknesses are obtained. At high cutting speed, the maximum WL thickness is obtained while the minimum forces are reached. The minimum WL thickness and the maximum forces are obtained when the depth of cut is maximized (4 mm in the experiment).

Figure 8 (d–f) shows also the interaction effect plots of the input factors on machining forces and WL thickness. The importance of interaction effects is observed graphically by means of the slope of the lines. It is noticed that all the combination interactions contribute to the desired responses. The effect of interaction between the cutting speed and feed rate on the WL thickness seems to be dominant compared to the other interactions. Otherwise, essentially, the interaction between the feed rate and the depth of cut has an important effect on the machining forces. The interaction between the feed and the cutting speed shows a decreasing trend. Nerveless, this interaction is not as significant as compared with the other interactions.

6 Optimization of hard turning conditions

6.1 Optimization

The response objectives are dependent on the requirements of a particular application. In order to obtain the required product quality, the optimal combination of factors for cutting AISI 52100 steel (62 HRc) are those minimizing machining force components and WL thickness. The cutting parameters that lead to achieve these objectives should be identified. Their identification is realized by means of the desirability function. This function ranges from zero (outside limits) to one (ideal case) and allows to find the optimal set of cutting parameters. The desirability function is defined as the weighted mean of the individual desirability functions and should be maximized. Figure 9 reveals the RSM optimization results. The optimized machining forces are Fc = 214 N and Ft = 180 N and the optimized WL thickness is 0.98 μm. These results are obtained with an overall desirability "D" equal to 0.9 and the corresponding optimum process parameters, cutting speed, feed rate, and depth of cut, are equal to 100 m/min, 0.06 mm/rev, and 1 mm, respectively.

6.2 Confirmation tests

To ensure the adequacy of the optimal hard turning operating parameters, a confirmation test is performed in the finite element model. It was revealed that when we use the optimal conditions (cutting speed, feed rate, depth of cut = 100 m/min, 0.06 mm/rev, 1 mm, respectively), the WL thickness is equal to 1 μm, the Fc is equal to 210 N, and the Ft is equal to 165 N.

7 Conclusion

In this paper, a finite element model (FEM) is developed in order to predict the machining forces and the WL thickness induced by orthogonal cutting of AISI52100 steel (62 HRc). The numerical study is followed by a statistical treatment of data in order to optimize the hard turning process. First, empirical models for predicting machining forces and WL thickness are developed based on the response surface methodology (RSM). The models, which are a second-order equations relating the desired responses to the process parameters (cutting speed, feed rate, and depth of cut), presented good fitting results. These empirical models have the advantage of calculating the WL thickness and the machining forces without the use of experimental procedures or the finite element simulations. Afterwards, the effects and interactions of input parameters are investigated by means of the analysis of variance (ANOVA). It is found that increasing the feed rate promotes the machining forces and the WL thickness. Nevertheless, increasing the cutting speed leads to a drop in machining forces and an increase in the WL thickness while increasing the depth of cut leads to a significant rise in the machining forces and a negligible decrease of the WL thickness. Lastly, the response optimizer tool is used in order to identify the set of process parameters that minimize both machining forces and WL thickness.

References

1. Ventura CE, Breidenstein B, Denkena B (2017) Influence of customized cutting edge geometries on the workpiece residual stress in hard turning. Proc Inst Mech Eng B J Eng Manuf, p. 95440541668538.
2. Zhao T, Zhou JM, Bushlya V, Stahl JE (2017) Effect of cutting edge radius on surface roughness and tool wear in hard turning of AISI 52100 steel. Int J Adv Manuf Technol:1–8
3. Shalaby MA, El Hakim MA, Veldhuis SC, Dosbaeva GK (2017) An investigation into the behavior of the cutting forces in precision turning. Int J Adv Manuf Technol 90(5–8):1605–1615
4. Chen T, Qiu C, Liu X, Qian X, Liu G (2017) Study on test method of white layer microhardness in hard cutting based on chord tangent method. Int J Adv Manuf Technol
5. Yan H, Hua J, Shivpuri R (2005) Numerical simulation of finish hard turning for AISI H13 die steel. Sci Technol Adv Mater 6(5): 540–547
6. Gaitonde VN, Karnik SR, Figueira L, Paulo Davim J (2009) Machinability investigations in hard turning of AISI D2 cold work tool steel with conventional and wiper ceramic inserts. Int J Refract Met Hard Mater 27(4):754–763
7. Zhang X-M, Chen L, Ding H (2016) Effects of process parameters on white layer formation and morphology in hard turning of AISI52100 steel. J Manuf Sci Eng 138(7):74502
8. Arfaoui S, Zemzemi F, Tourki Z (2018) A numerical-analytical approach to predict white and dark layer thickness of hard machining. Int J Adv Manuf Technol, https://doi.org/10.1007/s00170-018-1831-2
9. Saini S, Ahuja IS, Sharma VS (2012) Influence of cutting parameters on tool wear and surface roughness in hard turning of AISI H11 tool steel using ceramic tools. Int J Precis Eng Manuf 13(8):1295–1302
10. Das SR, Dhupal D, Kumar A (2015) Study of surface roughness and flank wear in hard turning of AISI 4140 steel with coated ceramic inserts. J Mech Sci Technol 29(10):4329–4340
11. Lalwani DI, Mehta NK, Jain PK (2008) Experimental investigations of cutting parameters influence on cutting forces and surface roughness in finish hard turning of MDN250 steel. J Mater Process Technol 206(1–3):167–179
12. Bouacha K, Yallese MA, Mabrouki T, Rigal JF (2010) Statistical analysis of surface roughness and cutting forces using response surface methodology in hard turning of AISI 52100 bearing steel with CBN tool. Int J Refract Met Hard Mater 28(3):349–361
13. Özel T, Hsu TK, Zeren E (2005) Effects of cutting edge geometry, workpiece hardness, feed rate and cutting speed on surface roughness and forces in finish turning of hardened AISI H13 steel. Int J Adv Manuf Technol 25(3–4):262–269
14. Kartal ME, Başağa HB, Bayraktar A (2011) Probabilistic nonlinear analysis of CFR dams by MCS using response surface method. Appl Math Model 35(6):2752–2770
15. Johnson GR, Cook WH (1985) Fracture characteristics of three metals subjected to various strains, strain rates, temperatures and pressures. Eng Fract Mech 21(1):31–48

16. Duan C, Kong W, Hao Q, Zhou F (2013) Modeling of white layer thickness in high speed machining of hardened steel based on phase transformation mechanism. Int J Adv Manuf Technol 69(1–4):59–70
17. Shi J, Liu CR (2006) On predicting chip morphology and phase transformation in hard machining. Int J Adv Manuf Technol 27(7–8):645–654
18. Zhang X, Wu S, Wang H, Liu CR (2011) Predicting the effects of cutting parameters and tool geometry on hard turning process using finite element method. J Manuf Sci Eng 133(4):41010
19. Din SKS, Ricottura FN, Rinvenimento T Comparable standards. pp. 91–92.
20. Ramesh A, Melkote SN (2008) Modeling of white layer formation under thermally dominant conditions in orthogonal machining of hardened AISI 52100 steel. Int J Mach Tools Manuf 48(3–4):402–414
21. Hua J, Umbrello D, Shivpuri R (2006) Investigation of cutting conditions and cutting edge preparations for enhanced compressive subsurface residual stress in the hard turning of bearing steel. J Mater Process Technol 171(2):180–187
22. Chou YK, Song H (2005) Thermal modeling for white layer predictions in finish hard turning. Int J Mach Tools Manuf 45(4–5):481–495